Channel Rank Analysis of an Outdoor-to-Indoor Massive MIMO Measurement

Daniel Schützenhöfer*†, Stefan Pratschner*†, Herbert Groll† and Markus Rupp†
*Christian Doppler Laboratory for Dependable Wireless Connectivity for the Society in Motion
†Institute of Telecommunications, TU Wien, Austria

***Abstract*—Massive multiple-input multiple-output (MIMO) communication often assumes propagation with a dense scattering environment. In this context, we performed an outdoor-to indoor massive MIMO channel measurement. To analyze the multipath components (MPCs) we apply the concept of a double directional radio channel. We evaluate the two-dimensional angular power-spectral density, which shows the amount of power that was carried over a certain Direction of Departure (DOD) - Direction of Arrival (DOA) pair. The estimation of the angular power-spectral density is achieved by an conventional beamformer. The beamforming results lead to the conclusion that the channel may be described by a low number of MPCs. To analyze the rank of the wireless channel, we compare the achievable rate for the measured channel with low rank approximated versions. The result shows that the measured outdoor-to-indoor MIMO channel is approximated well with a low rank channel model.**

***Index Terms*—massive MIMO, virtual antenna array, outdoor-to-indoor measurement, double directional beamforming**

I. Introduction

Massive multiple-input multiple-output (MIMO) is a major component for the next-generation of wireless communications. This technology greatly improves the capacity, spectral efficiency, robustness and reliability of wireless systems [1], [2]. To achieve those benefits, so called favorable propagation conditions must hold [1]. To investigate the performance of massive MIMO channels in real propagation environments, measurement campaigns with large antenna arrays were performed [3], [4]. As a high number of antennas leads to an increasing hardware complexity of MIMO channel measurements often the concept of virtual antenna array is employed [5]–[7]. Virtual antenna array measurements are performed in stationary environments. A single antenna is mounted on an mechanical guide system and is moved to different positions in between measurements to form a virtual antenna array. Since only one antenna position is measured at a time, the whole measurement setup needs to be time-invariant. This means the measured wireless channel, which is part of the investigation needs to be static and also the hardware at the receiver and transmitter have to be time-invariant [8], [9]. Typically a rich scattering environment is assumed for an indoor user. Therefore, user channels are often modeled considering an independent, identically distributed (i.i.d.) Rayleigh fading channel model [10], [11]. In [12], the authors characterized an outdoor-to-indoor scenario by a rich multipath fading model. An outdoor-to-indoor double directional measurement campaign in [13] shows that the angular dispersion at the outdoor link end is rather small, but at the indoor link side significant energy arrives from all directions.

The financial support by the Austrian Federal Ministry for Digital and Economic Affairs and the National Foundation for Research, Technology and Development is gratefully acknowledged.

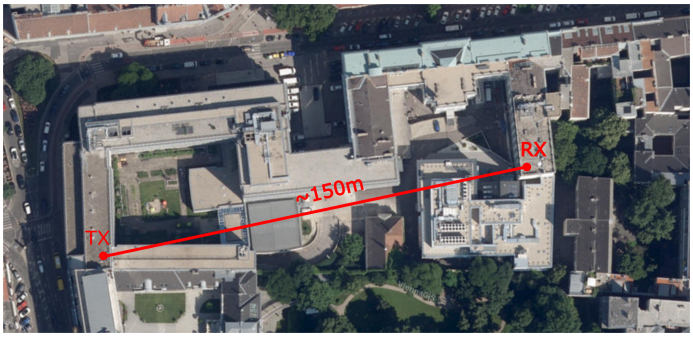

Fig. 1. Areal photo of the measurement scenario [14]. The transmitter is located outdoor at the rooftop. The receive antenna is indoor in an office environment.

Contribution: We perform massive MIMO outdoor-to-indoor channel measurements with virtual arrays at transmitter and receiver side. In this contribution, we firstly focus on the estimation of the Direction of Arrival (DOA) and Direction of Departure (DOD). From this observation we conclude that only a few propagation paths are dominant. Then, secondly, we compare our measurements with a low rank double-sided massive MIMO channel model.

II. Measurement Setup

For our measurement, virtual antenna arrays at transmitter and receiver side are applied. The measuring setup consists of a transmit (TX) antenna which is placed outdoor on a rooftop and a receive (RX) antenna which is located indoor in an office environment. The measurement environment is shown in Fig. 1. The center frequency of our measurement is $2.5\,\mathrm{GHz}$.

The TX antenna is a printed dipole antenna which is mounted in front of a $6.25\lambda \times 6.25\lambda$ large quadratic aluminum reflector plate. This antenna design yields a directional antenna pattern with a gain of $6\,\mathrm{dBi}$. The measurement setup shown in Fig. 2 allows us to move the TX antenna in y and z direction. For our measurement we generate a $N_{t,y} = 40$ times $N_{t,z} = 7$ vertical virtual uniform

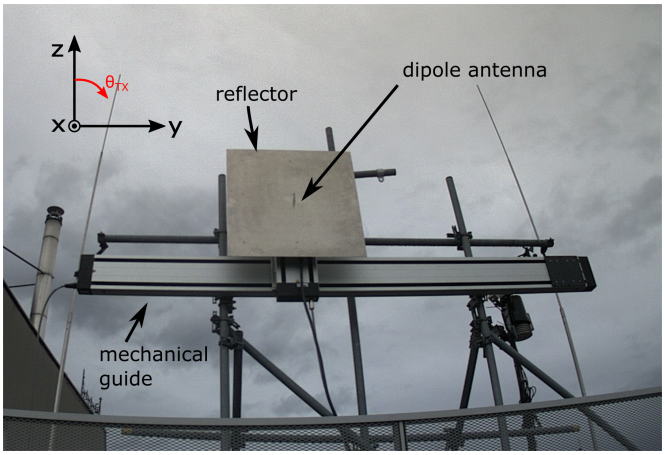

Fig. 2. Setup at the transmitter for virtual antenna array measurements. The mounted antenna can be moved in y and z direction.

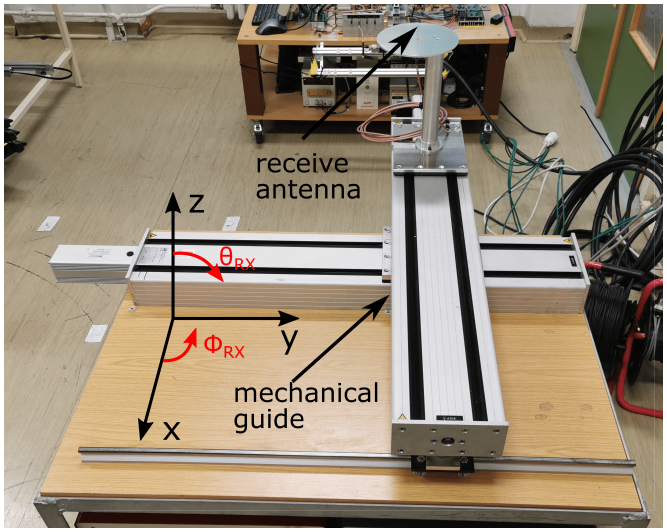

Fig. 3. Setup at the receiver for virtual antenna array measurements. The mounted antenna can be moved in x and y direction.

planar array with an antenna spacing of $d = 0.5\lambda$. At the transmitter there is a total number of $N_t = 280$ different antenna positions.

To enable spatial analysis of the multipath components (MPCs) in terms of DOA estimation, we employ a large antenna array at the receiver side. The RX antenna is a $\lambda/4$ monopol antenna mounted indoor on a XY positioning table in an office environment, shown in Fig. 3. By moving the antenna to $N_r = 169$ different positions we form a $N_{r,x} = 13$ times $N_{r,y} = 13$ horizontal virtual uniform planar antenna array with a spacing of $d = 0.5\lambda$.

Transmit Signal

As a transmit signal, we consider an orthogonal frequency division multiplexing (OFDM) signal with a center frequency of approx. 2.5 GHz. To obtain a low crest factor, Newman Phases were applied [15]. The transmit signal is described by [16]

$$x(n) = \mathrm{Re}\left(\sum_{k=-K/2}^{K/2-1} \mathrm{e}^{-j2\pi k \frac{n}{N}} \mathrm{e}^{j\pi \frac{k^2}{K}} \right), \qquad (1)$$

where $n = 0, 1, \ldots, N-1$ is the time index and K is the number of subcarriers. For our measurements we chose $K = 100$ subcarriers. A subcarrier spacing of 15 kHz leads to a total bandwidth of $100 \times 15\,\mathrm{kHz} = 1.5\,\mathrm{MHz}$. Each transmit sequence consists of 100 symbols. Assuming a time-invariant channel, averaging over 100 received symbols leads to a processing gain of 20 dB. The transmit sequence is transmitted once for each antenna position of the virtual arrays. We obtain the channel estimates by least squares channel estimation. Since the channel is sufficiently flat in the frequency domain we average the channel estimates over the subcarriers. This further improves the quality of the channel estimates.

III. Double Directional Beamforming

To analyze the MPCs of the massive MIMO channel we apply the concept of a double directional radio channel [17].

From our measurement we obtain the MIMO channel matrix $\mathbf{H} \in \mathbb{C}^{N_r \times N_t}$ with complex channel coefficients.

We now estimate the angular power spectrum by applying a conventional beamformer as follows [18]

$$P_{\mathrm{BF}}(\Phi_{\mathrm{Rx}}, \theta_{\mathrm{Rx}}, \Phi_{\mathrm{Tx}}, \theta_{\mathrm{Tx}}) = |\mathbf{a}_{\mathrm{Rx}}^{\mathrm{H}}(\Phi_{\mathrm{Rx}}, \theta_{\mathrm{Rx}})\, \mathbf{H}\, \mathbf{a}_{\mathrm{Tx}}(\Phi_{\mathrm{Tx}}, \theta_{\mathrm{Tx}})|^2, \qquad (2)$$

where $(\cdot)^{\mathrm{H}}$ denotes the Hermitian transpose and $\mathbf{a}_{\mathrm{Rx}}(\Phi_{\mathrm{Rx}}, \theta_{\mathrm{Rx}})$ and $\mathbf{a}_{\mathrm{Tx}}(\Phi_{\mathrm{Tx}}, \theta_{\mathrm{Tx}})$ are the steering vectors at the receiver and transmitter. The steering vector $\mathbf{a}_{\mathrm{Rx}}(\Phi_{\mathrm{Rx}}, \theta_{\mathrm{Rx}})$ of a **horizontal** uniform rectangular array is expressed as [19]

$$\mathbf{a}_{\mathrm{Rx}}(\Phi_{\mathrm{Rx}}, \theta_{\mathrm{Rx}}) = \mathbf{a}_{\mathrm{Rx,y}}(\Phi_{\mathrm{Rx}}, \theta_{\mathrm{Rx}}) \otimes \mathbf{a}_{\mathrm{Rx,x}}(\Phi_{\mathrm{Rx}}, \theta_{\mathrm{Rx}}), \qquad (3)$$

where $\otimes$ denotes the Kronecker product, $\mathbf{a}_{\mathrm{Rx,x}}(\Phi_{\mathrm{Rx}}, \theta_{\mathrm{Rx}})$ is the steering vector in x direction and $\mathbf{a}_{\mathrm{Rx,y}}(\Phi_{\mathrm{Rx}}, \theta_{\mathrm{Rx}})$ is the steering vector in y direction. The steering vectors $\mathbf{a}_{\mathrm{Rx,x}}(\Phi_{\mathrm{Rx}}, \theta_{\mathrm{Rx}})$ and $\mathbf{a}_{\mathrm{Rx,y}}(\Phi_{\mathrm{Rx}}, \theta_{\mathrm{Rx}})$ take on the form

$$\mathbf{a}_{\mathrm{Rx,x}}(\Phi_{\mathrm{Rx}}, \theta_{\mathrm{Rx}}) = \begin{bmatrix} 1 & \mathrm{e}^{ju_x} & \ldots & \mathrm{e}^{j(N_{r,x}-1)u_x} \end{bmatrix}^{\mathrm{T}}, \qquad (4)$$

$$\mathbf{a}_{\mathrm{Rx,y}}(\Phi_{\mathrm{Rx}}, \theta_{\mathrm{Rx}}) = \begin{bmatrix} 1 & \mathrm{e}^{ju_y} & \ldots & \mathrm{e}^{j(N_{r,y}-1)u_y} \end{bmatrix}^{\mathrm{T}}, \qquad (5)$$

where u_x and u_y are especially simple for a spacing of $d = 0.5\,\lambda$

$$u_x = \frac{\omega}{c} d \cos(\Phi_{\mathrm{Rx}}) \sin(\theta_{\mathrm{Rx}}) = \pi \cos(\Phi_{\mathrm{Rx}}) \sin(\theta_{\mathrm{Rx}}), \qquad (6)$$

$$u_y = \frac{\omega}{c} d \sin(\Phi_{\mathrm{Rx}}) \sin(\theta_{\mathrm{Rx}}) = \pi \sin(\Phi_{\mathrm{Rx}}) \sin(\theta_{\mathrm{Rx}}). \qquad (7)$$

Here ω denotes the angular frequency and c denotes the speed of light. The steering vector $\mathbf{a}_{\mathrm{Tx}}(\Phi_{\mathrm{Tx}}, \theta_{\mathrm{Tx}})$ of a **vertical** uniform rectangular array is written as

$$\mathbf{a}_{\mathrm{Tx}}(\Phi_{\mathrm{Tx}}, \theta_{\mathrm{Tx}}) = \mathbf{a}_{\mathrm{Tx,z}}(\Phi_{\mathrm{Tx}}, \theta_{\mathrm{Tx}}) \otimes \mathbf{a}_{\mathrm{Tx,y}}(\Phi_{\mathrm{Tx}}, \theta_{\mathrm{Tx}}), \qquad (8)$$

where $\mathbf{a}_{\mathrm{Tx,y}}(\Phi_{\mathrm{Tx}}, \theta_{\mathrm{Tx}})$ and $\mathbf{a}_{\mathrm{Tx,z}}(\Phi_{\mathrm{Tx}}, \theta_{\mathrm{Tx}})$ are the steering vector in y and z direction and defined as

$$\mathbf{a}_{\mathrm{Tx,y}}(\Phi_{\mathrm{Tx}}, \theta_{\mathrm{Tx}}) = \begin{bmatrix} 1 & \mathrm{e}^{jv_y} & \dots & \mathrm{e}^{j(N_{t,y}-1)v_y} \end{bmatrix}^{\mathrm{T}}, \quad (9)$$

$$\mathbf{a}_{\mathrm{Tx,z}}(\Phi_{\mathrm{Tx}}, \theta_{\mathrm{Tx}}) = \begin{bmatrix} 1 & \mathrm{e}^{jv_z} & \dots & \mathrm{e}^{j(N_{t,z}-1)v_z} \end{bmatrix}^{\mathrm{T}}, \quad (10)$$

where v_y and v_z are especially simple for a spacing of $d = 0.5\,\lambda$

$$v_y = \frac{\omega}{c}\, d \sin(\Phi_{\mathrm{Tx}})\sin(\theta_{\mathrm{Tx}}) = \pi \sin(\Phi_{\mathrm{Tx}})\sin(\theta_{\mathrm{Tx}}), \quad (11)$$

$$v_z = \frac{\omega}{c}\, d \cos(\theta_{\mathrm{Tx}}) \qquad = \pi \cos(\theta_{\mathrm{Tx}}). \quad (12)$$

Since TX and RX are approximately at the same height, we expect the dominant paths at an elevation angle of 90°. One realization of the resulting discrete two-dimensional angular power-spectral density at a DOD elevation of $\theta_{\mathrm{Tx}} = 90°$ and a DOA elevation of $\theta_{\mathrm{Rx}} = 90°$ is depicted in Fig. 4. It evaluates the amount of power that was carried over a certain DOA-DOD pair. We generate a uniform planar array at the receiver to determine the azimuth DOA unambiguously. The figure shows that there are two dominant DOA-DOD pairs. Analyzing other DOA/DOD elevation values showed that there are no other dominant paths at elevation angles different from 90°. That leads to the conclusion that the channel may be described by a small number of MPCs although this is not typical for a indoor environment.

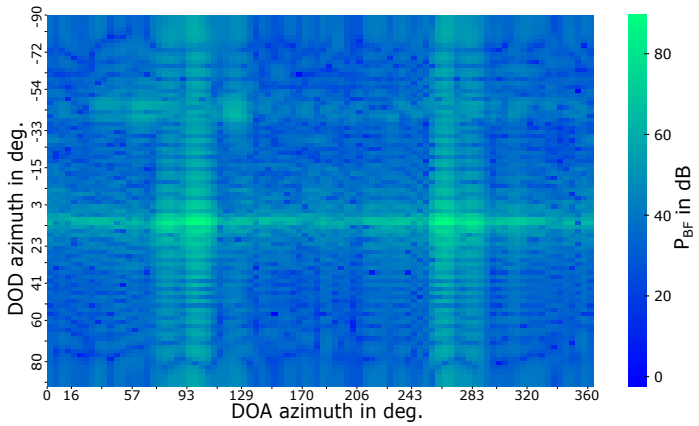

Fig. 4. Discrete two-dimensional angular power-spectral density at a DOD elevation of $\theta_{\mathrm{Tx}} = 90°$ and a DOA elevation of $\theta_{\mathrm{Rx}} = 90°$.The strongest components are located at a DOD azimuth of 13°.

IV. Channel Model

We approximate the measured channel by employing the double-sided massive MIMO narrow-band clustered channel model with L different channel paths. The channel matrix $\mathbf{H}_{\mathrm{sim}}$ can be written as [20]

$$\mathbf{H}_{\mathrm{sim}} = \sqrt{\frac{1}{L}} \sum_{l=1}^{L} \alpha_l \mathbf{a}_{\mathrm{Rx}}(\Phi_{\mathrm{Rx},l}, \theta_{\mathrm{Rx},l}) \mathbf{a}_{\mathrm{Tx}}^{\mathrm{T}}(\Phi_{\mathrm{Tx},l}, \theta_{\mathrm{Tx},l}), \quad (13)$$

where α_l is the complex channel gain of path l and corresponding steering vectors $\mathbf{a}_{\mathrm{Rx}}(\Phi_{\mathrm{Rx},l}, \theta_{\mathrm{Rx},l})$, $\mathbf{a}_{\mathrm{Tx}}(\Phi_{\mathrm{Tx},l}, \theta_{\mathrm{Tx},l})$ at RX and TX. The channel rank of the matrix $\mathbf{H}_{\mathrm{sim}}$ depends on the angular distribution of the paths. Generating L independent paths and assuming that $L \leq \min(N_r, N_t)$ leads to $\mathrm{rank}(\mathbf{H}_{\mathrm{sim}}) = L$ with probability 1 [20].

For an approximation of the measured channel with only a few MPCs, we need to evaluate the strongest L paths of the measurement. Therefore, we calculate the absolute value of the beamformer result (2) and sort it in descending order. The corresponding parameters α_l, $\Phi_{\mathrm{Rx},l}$, $\theta_{\mathrm{Rx},l}$, $\Phi_{\mathrm{Tx},l}$ and $\theta_{\mathrm{Tx},l}$ of the L strongest paths are applied onto our channel model in (13). That allows us to approximate the measured channel matrix with different number of MPCs.

V. MIMO channel rank analysis

To analyze the rank of the measured channel matrix we applied the singular value decomposition to $\mathbf{H}_{\mathrm{meas}}\mathbf{H}_{\mathrm{meas}}{}^{\mathrm{H}}$. The first 50 largest singular values are shown in Fig. 5. Similarly we plot the singular values of a simulated channel matrix as in Section IV with $L = 15$ paths. All singular values are normalized to the strongest one of the measurement. Although the singular values of the measured channel matrix decrease rapidly, the measured channel matrix has full rank. Only the six largest singular values lie in a range of 30 dB. The simulated channel matrix shows L non-zero singular values.

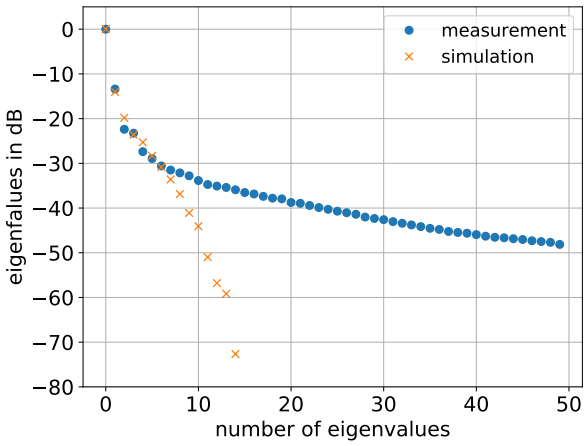

Fig. 5. Singular values of the measured channel and a simulated channel with 15 paths. The measured channel has full rank but the singular values decrease rapidly.

To analyze the number of dominant paths we compare the channel capacities of the measured channel with simulated double-sided MIMO channels containing a different number of paths. In the high signal-to-noise ratio (SNR) regime the achievable rate scales asymptotically with the channel rank. We calculate the achievable rate for the channel as [21]

$$C = \log_2 \left(\det(\mathbf{I}_{N_r} + \frac{P}{\sigma^2 N_t} \mathbf{H}\mathbf{H}^{\mathrm{H}}) \right) \text{ in bit/s/Hz}, \quad (14)$$

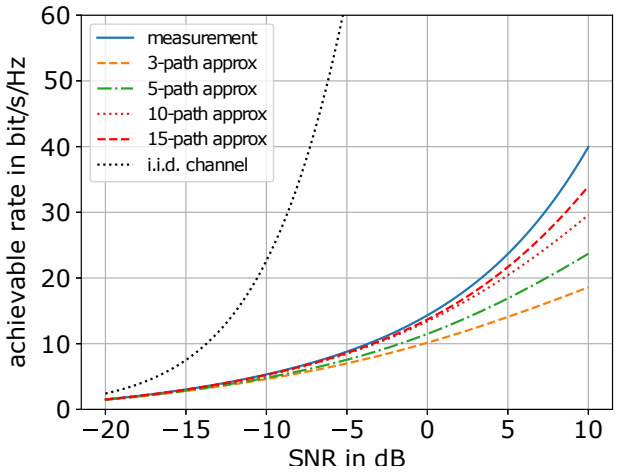

Fig. 6. Achievable rate for the measured channel and the achievable rate for approximations with various rank. At low SNR only a few MPCs are needed to reach the measurement. At high SNR more propagation paths are needed.

where $\mathbf{I}_{N_r}$ is the $N_r \times N_r$ identity matrix, P is the total transmit power and σ^2 is the noise power. For ease of analysis, the channel matrix $\mathbf{H}$ is normalized such that [22]

$$\frac{1}{N_r N_t}\left(\sum_{i=1}^{N_r}\sum_{j=1}^{N_t}|h_{ij}|^2\right) = 1, \tag{15}$$

where h_{ij} denotes the ith row and jth column entry of the channel matrix $\mathbf{H}$.

The normalization of the channel matrix leads to

$$C = \log_2\left(\det(\mathbf{I}_{N_r} + \frac{\rho}{N_t}\hat{\mathbf{H}}\hat{\mathbf{H}}^{\mathrm{H}})\right) \text{ in bit/s/Hz}, \tag{16}$$

where $\hat{\mathbf{H}}$ is the normalized channel matrix and $\rho = {}^{P}/_{\sigma^2}$ is the average received SNR. Figure 6 shows the achievable rate for the measured channel and the achievable rate for approximations with various rank. By adding more MPCs in our simulated channel, the achievable rate and the slope at high SNR increases which is a direct consequence of adding more paths to our simulation. In comparison to the measured channel the achievable rate for an i.i.d. Rayleigh channel increases fast, because all singular values of the i.i.d. channel have about the same strength. For means of demonstration we calculate the achievable rate approximation error at different SNR as

$$\mathrm{err}(\rho) = \frac{|C_{\mathrm{meas}}(\rho) - C_i(\rho)|}{C_{\mathrm{meas}}(\rho)}, \tag{17}$$

where C_i is the achievable rate for the approximation with a number of i propagation paths and C_{meas} is the achievable rate for the measured channel. We utilize the error function (17) to compare the achievable rate for the measured channel C_{meas} with the achievable rate for an approximated channel C_i containing $i = 15$ MPCs. The result is shown in Fig. 7. At a low SNR the achievable rate for the approximation is close to the achievable rate for measurement. In an area of -20 to -5 dB the error is below 2%. In this case only the dominant paths are decisive. For a higher SNR the error is increasing fast. At high SNR we need more non-zero singular values to describe the channel. Therefore, more independent MPCs are needed to reach the achievable rate for the measured channel. A channel approximation with 15 MPCs shows an error of 15% at a SNR of 10 dB. Please note that the SNR without array gain is typically low in a massive MIMO system. For example, authors in [23] assume an SNR of -5 dB for their simulations. This is reasonable, since $N_t = 280$ transmit antennas result in an array gain of approx 24.5 dB.

We conclude that the a channel approximation with a low number of propagation paths leads to a very good fit with the measurement in terms of achievable rate at low SNR. To fit the measurement perfectly at high SNR we theoretically need a total number of 169 independent paths. In comparison to the 169 paths our result shows that we need a relatively small number of MPCs to achieve a good channel approximation also in the high SNR domain.

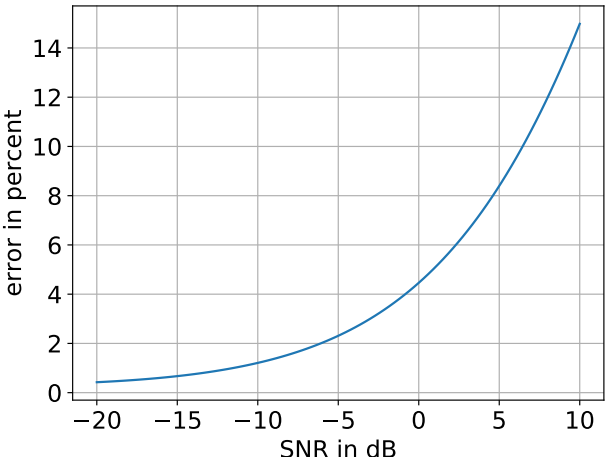

Fig. 7. Error function of the measured channel and an approximated channel containing $i = 15$ MPCs.

VI. Conclusion

In this contribution, we approximate a measured outdoor-to-indoor massive MIMO channel with a small number of MPCs. A two-dimensional angular power-spectral density estimation leads to the conclusion that, unlike the natural assumption of a high number of propagation paths in a dense scattering environment, we only have a low number of dominant MPCs. The singular values of the measured channel show that the channel matrix has full rank but only the six largest singular values lie in a range of 30 dB. At low SNR our channel approximation leads to a very good fit with the measurement in terms of achievable rate. In comparison to the theoretically predicted 169 independent MPCs, we only need a small number of propagation paths to approximate the channel well.

REFERENCES

[1] E. G. Larsson, O. Edfors, F. Tufvesson, and T. L. Marzetta, "Massive MIMO for next generation wireless systems," *IEEE Communications Magazine*, vol. 52, no. 2, pp. 186–195, February 2014.

[2] X. Zhao, P. Jia, Q. Zhang, Y. Li, R. Xing, and Y. Liu, "Analysis of a distributed MIMO channel capacity under a special scenario," *EURASIP Journal on Wireless Communications and Networking*, vol. 2019, 12 2019.

[3] X. Gao, O. Edfors, F. Rusek, and F. Tufvesson, "Massive MIMO performance evaluation based on measured propagation data," *IEEE Transactions on Wireless Communications*, vol. 14, no. 7, pp. 3899–3911, July 2015.

[4] X. Gao, O. Edfors, F. Rusek, and F. Tufvesson, "Linear pre-coding performance in measured very-large MIMO channels," in *2011 IEEE Vehicular Technology Conference (VTC Fall)*. IEEE, 2011, pp. 1–5.

[5] J. Hoydis, C. Hoek, T. Wild, and S. ten Brink, "Channel measurements for large antenna arrays," in *2012 International Symposium on Wireless Communication Systems (ISWCS)*, August 2012, pp. 811–815.

[6] D. Schützenhöfer, E. Zöchmann, M. Lerch, S. Pratschner, H. Groll, S. Caban, and M. Rupp, "Experimental evaluation of the influence of fast movement on virtual antenna arrays," in *WSA 2019; 23rd International ITG Workshop on Smart Antennas*. VDE, 2019, pp. 1–5.

[7] J. Huang, C. Wang, R. Feng, J. Sun, W. Zhang, and Y. Yang, "Multi-frequency mmWave massive MIMO channel measurements and characterization for 5G wireless communication systems," *IEEE Journal on Selected Areas in Communications*, vol. 35, no. 7, pp. 1591–1605, July 2017.

[8] N. Czink, B. Bandemer, G. Vazquez-Vilar, L. Jalloul, and A. Paulraj, "Can multi-user MIMO measurements be done using a single channel sounder?" in *Proc. COST 2100 6th Manage. Committee Meeting*, 2008, pp. 6–8.

[9] D. S. Baum and H. Bölcskei, "Impact of phase noise on MIMO channel measurement accuracy," in *IEEE 60th Vehicular Technology Conference, 2004. VTC2004-Fall. 2004*, vol. 3. IEEE, 2004, pp. 1614–1618.

[10] G. J. Foschini and M. J. Gans, "On limits of wireless communications in a fading environment when using multiple antennas," *Wireless personal communications*, vol. 6, no. 3, pp. 311–335, 1998.

[11] K. Zheng, S. Ou, and X. Yin, "Massive MIMO channel models: A survey," *International Journal of Antennas and Propagation*, vol. 2014, 2014.

[12] C. Hermosilla, R. Feick, R. A. Valenzuela, and L. Ahumada, "Improving MIMO capacity with directive antennas for outdoor-indoor scenarios," in *VTC Spring 2008 - IEEE Vehicular Technology Conference*, May 2008, pp. 414–418.

[13] S. Wyne, A. F. Molisch, P. Almers, G. Eriksson, J. Karedal, and F. Tufvesson, "Outdoor-to-indoor office MIMO measurements and analysis at 5.2 GHz," *IEEE Transactions on Vehicular Technology*, vol. 57, no. 3, pp. 1374–1386, May 2008.

[14] Stadt Wien - ViennaGIS. [Online]. Available: www.wien.gv.at/viennagis/

[15] E. Zöchmann, C. F. Mecklenbräuker, M. Lerch, S. Pratschner, M. Hofer, D. Löschenbrand, J. Blumenstein, S. Sangodoyin, G. Artner, S. Caban, T. Zemen, A. Prokeš, M. Rupp, and A. F. Molisch, "Measured delay and Doppler profiles of overtaking vehicles at 60 GHz," in *12th European Conference on Antennas and Propagation (EuCAP 2018)*, April 2018, pp. 1–5.

[16] S. Pratschner, S. Caban, D. Schützenhöfer, M. Lerch, E. Zöchmann, and M. Rupp, "A fair comparison of virtual to full antenna array measurements," in *2018 IEEE 19th International Workshop on Signal Processing Advances in Wireless Communications (SPAWC)*. IEEE, 2018, pp. 1–5.

[17] M. Steinbauer, A. F. Molisch, and E. Bonek, "The double-directional radio channel," *IEEE Antennas and Propagation Magazine*, vol. 43, no. 4, pp. 51–63, Aug 2001.

[18] H. Krim and M. Viberg, "Two decades of array signal processing research: the parametric approach," *IEEE signal processing magazine*, vol. 13, no. 4, pp. 67–94, 1996.

[19] X. He and Z. Zhang, "DOA estimation with uniform rectangular array in the presence of mutual coupling," in *2nd IEEE International Conference on Computer and Communications (ICCC)*, 2016, pp. 1854–1859.

[20] L. N. Ribeiro, S. Schwarz, and A. L. De Almeida, "Double-sided massive MIMO transceivers for mmWave communications," *IEEE Access*, vol. 7, pp. 157 667–157 679, 2019.

[21] B. Clerckx and C. Oestges, *MIMO Wireless Networks: Channels, Techniques and Standards for Multi-Antenna, Multi-User and Multi-Cell Systems*, 2nd ed. USA: Academic Press, Inc., 2013.

[22] X. Zhao, P. Jia, Q. Zhang, Y. Li, R. Xing, and Y. Liu, "Analysis of a distributed MIMO channel capacity under a special scenario," *EURASIP Journal on Wireless Communications and Networking*, vol. 2019, 12 2019.

[23] E. Björnson, E. G. Larsson, and T. L. Marzetta, "Massive MIMO: ten myths and one critical question," *IEEE Communications Magazine*, vol. 54, no. 2, pp. 114–123, Feb. 2016.